J. Plasma Physics (2009), *vol.* 75, *part* 3, *pp.* 303–318.
doi:10.1017/S0022377808007526 Printed in the United Kingdom

Stochastic layer scaling in the two-wire model for divertor tokamaks

HALIMA ALI[1], ALKESH PUNJABI[1]
and ALLEN BOOZER[2]

[1]Hampton University, Hampton, VA 23668, USA
(halima.ali@hamptonu.edu)

[2]Columbia University, New York, NY 10027, USA

(Received 11 April 2008 and in revised form 9 July 2008, first published online 18 August 2008)

Abstract. The question of magnetic field structure in the vicinity of the separatrix in divertor tokamaks is studied. The authors have investigated this problem earlier in a series of papers, using various mathematical techniques. In the present paper, the two-wire model (TWM) [Reiman, A. 1996 *Phys. Plasmas* **3**, 906] is considered. It is noted that, in the TWM, it is useful to consider an extra equation expressing magnetic flux conservation. This equation does not add any more information to the TWM, since the equation is derived from the TWM. This equation is useful for controlling the step size in the numerical integration of the TWM equations. The TWM with the extra equation is called the flux-preserving TWM. Nevertheless, the technique is apparently still plagued by numerical inaccuracies when the perturbation level is low, resulting in an incorrect scaling of the stochastic layer width. The stochastic broadening of the separatrix in the flux-preserving TWM is compared with that in the low mn (poloidal mode number m and toroidal mode number n) map (LMN) [Ali, H., Punjabi, A., Boozer, A. and Evans, T. 2004 *Phys. Plasmas* **11**, 1908]. The flux-preserving TWM and LMN both give Boozer–Rechester 0.5 power scaling of the stochastic layer width with the amplitude of magnetic perturbation when the perturbation is sufficiently large [Boozer, A. and Rechester, A. 1978, *Phys. Fluids* **21**, 682]. The flux-preserving TWM gives a larger stochastic layer width when the perturbation is low, while the LMN gives correct scaling in the low perturbation region. Area-preserving maps such as the LMN respect the Hamiltonian structure of field line trajectories, and have the added advantage of computational efficiency. Also, for a $1\frac{1}{2}$ degree of freedom Hamiltonian system such as field lines, maps do not give Arnold diffusion.

1. Introduction

The plasmas in modern tokamaks are bounded by the separatrix between magnetic field lines that form toroidal magnetic surfaces, on which plasma is confined, and open field lines that divert the plasma exhaust to divertor plates [1]. An ideal tokamak is axisymmetric, and the separatrix in an ideal tokamak is a sharp surface. Asymmetries in the magnetic field cause the last confining magnetic surface to lie inside the ideal separatrix and create a layer of open field lines between the last good surface and the ideal separatrix. This layer is called a stochastic layer. Near the X point, the width of the stochastic layer is proportional to the square root of the toroidally asymmetric part of the magnetic field [2]. The asymmetric

part of the magnetic field results from the field errors, plasma instabilities, or currents in external coils such as C coils or I coils in DIII-D [3] used to control stochasticity [4]. Magnetic field line trajectories are the trajectories of a $1\frac{1}{2}$ degree of freedom Hamiltonian [5,6]. Consequently, the tokamak separatrix and divertor are archetypal for the behavior of a region of bounded Hamiltonian trajectories surrounded by a region of open trajectories. The basic features of trajectories near a separatrix are generic for a Hamiltonian system. The study of magnetic field line behavior near the X point and the related plasma behavior are important for their application to tokamaks, to other Hamiltonian or near-Hamiltonian systems, and to the problem of heat deposition on collector plates [7].

The two-wire model (TWM) originated in a paper by Boozer and Rechester in 1978 [2]. In the TWM, two straight wires and a uniform axial magnetic field model the axisymmetric part of the magnetic field. The TWM is the simplest model that has the topology of divertor tokamaks. In 1996, Reiman investigated the TWM [8]. In Reiman's work, the equations for the trajectories of magnetic field lines in divertor tokamak are solved in cylindrical geometry. The ends of the cylinder are identified. An analytic term represents the field errors. The analytic term can be Fourier decomposed into an infinite series in modified Bessel functions. The simplicity of the TWM allows fast numerical integration of a large number of field line trajectories over long distances. Singular surfaces and the magnetic footprint are calculated from the numerical integration of field line trajectories. In the Reiman TWM for the three-dimensional (3D) poloidal divertor, unstable closed magnetic field lines that follow the pitch of rational surfaces govern the magnetic reconnection. Magnetic asymmetry destroys the ideal separatrix and the neighboring flux surfaces. This allows the magnetic field lines in the destroyed surfaces to reach the collector plate. Reiman's 1996 TWM study [8] relates to the work of Lau and Finn [9] on 3D plasmoids reconnection in the Solar corona. Lau and Finn built their work on the earlier work of Stern [10] and Greene [11] on 3D reconnection.

In this paper, we add an extra equation to the TWM equations. This additional differential equation is an analytical expression for the preservation of magnetic flux. The additional equation allows us to control the step size of numerical integration of the TWM equations to achieve the desired accuracy in the preservation of magnetic flux. We call the TWM with the additional differential equation the flux-preserving TWM. We use the same analytic term in the flux-preserving TWM to represent the field errors. We use the flux-preserving TWM to calculate the magnetic structure of the stochastic layer and magnetic footprint in the divertor tokamaks. We calculate the properties of magnetic field lines in the stochastic layer and in the footprint, the structures of the stochastic layer near the X point, and the scaling of the width of the stochastic layer with the amplitude of the magnetic perturbation. We also compare the results of the flux-preserving TWM with the low mn (poloidal mode number m and toroidal mode number n) map (LMN). A comparison shows that even when an additional equation is added to the TWM for flux-preservation, we do not obtain correct scaling of the stochastic layer for small amplitudes of perturbation; however, the LMN gives the correct scaling while preserving the Hamiltonian structure.

2. The standard TWM

In this section, we give a brief description of the standard TWM [2,8]. The TWM is the simplest physical model that has the topology of divertor tokamaks. Full details

https://doi.org/10.1017/S0022377808007526 Published online by Cambridge University Press

of the standard TWM were given in [8]. In the standard TWM, a single, straight wire located at $x = 0$, $y = 1$ represents the plasma current. Another straight wire at $x = 0$, $y = -1$ creates a single-null divertor. Current in both of the wires is equal. A divertor plate is located at the $y = 0$ plane. The X point formed by the ideal separatrix surface runs along the $x = 0$ line on the plate. The unperturbed magnetic field is

$$\mathbf{B} = \mathbf{z} \times \nabla \boldsymbol{\Psi}_0 + B_0 \hat{z}, \tag{1}$$

where $\Psi_0 = C \log(r_\mathrm{p} r_\mathrm{c})$. Here r_p and r_c are distances from the two wires (see [8, Fig. 3]), $r_\mathrm{p}^2 = x^2 + (y-1)^2$ and $r_\mathrm{c}^2 = x^2 + (y+1)^2$ and C is a constant. It is proportional to the currents in the wires. A non-axisymmetric magnetic field,

$$\delta \mathbf{B} = \delta_\mathrm{T} B_0 \nabla \boldsymbol{\chi}, \tag{2}$$

where

$$\boldsymbol{\chi} = \left(\frac{1}{k}\right) \cos(kz) e^{kx} \tag{3}$$

is superimposed on the axisymmetric field produced by the two wires. Here δ_T is the amplitude of the magnetic perturbation. The subscript T denotes the TWM. This magnetic perturbation is both curl- and divergence-free. The periodicity length in the z direction is $L = 2\pi R$. Here R is the major radius of the tokamak. Since the distance from the wires to the X point is unity, R is approximately equal to the aspect ratio. In TWM, $R = 3$. The non-axisymmetric perturbation satisfies $k = n/R$. Here n is an integer. The constant C is chosen so that in the absence of the divertor coil the cylindrical safety factor $q = 3$ on the $r_\mathrm{p} = 1$ surface. This leads to $C = B_0/9$. The presence of the divertor coil in the tokamak creates an X point at the origin, and $q \to \infty$ as one approaches the X point. To compare the magnitudes of field errors in tokamaks, we can Fourier decompose the field error. For this purpose, a circular magnetic surface with center at the major radius is chosen as the reference surface, and the Fourier components of the perturbation are calculated from the expansion of the exponential term in (3) as

$$e^{k \cos\theta} = I_0(k) + \sum_{m=1}^{\infty} 2 I_m(k) \cos(m\theta). \tag{4}$$

Here I_m is the modified Bessel function of order m. In the outer midplane of the tokamak, $\theta = 0$, and with $n = 1$, $k = 1/3$, the modified Bessel functions $I_m(1/3)$ have the values $I_0(1/3) \cong 1.028$, $I_1(1/3) \cong 0.169$, $I_2(1/3) \cong 0.014$, and $I_3(1/3) \cong 0.0008$. For $n = 1$, the $m = 1, 2$, and 3 Fourier amplitudes of the perturbation $\delta B/B$ in the midplane are approximately $0.33\delta_\mathrm{T}$, $0.027\delta_\mathrm{T}$, and $0.0016\delta_\mathrm{T}$, respectively. In divertor tokamaks, the $n = 1$, $m = 2$ Fourier components of the field error are typically of the order of 10^{-4} times the toroidal magnetic field [12–14]. This corresponds roughly to the value $\delta_\mathrm{T} \approx 10^{-3}$ in the flux-preserving TWM. Here we set $k = 1/3$ and choose $\delta_\mathrm{T} = 10^{-3}$, the value used in [8]. We also choose the same value for the amplitude δ_M of the low mn perturbation in the LMN map. The subscript M in δ_M denotes the LMN as opposed to the subscript T that denotes the TWM.

To calculate the trajectories of the magnetic field lines, we numerically integrate the equations of motion of the magnetic field lines: $dx/dz = B_x/B_z$, and $dy/dz =$

https://doi.org/10.1017/S0022377808007526 Published online by Cambridge University Press

B_y/B_z. Finally, in the standard TWM, we numerically integrate the two equations

$$\frac{dx}{dz} = f(x, y, z), \tag{5}$$

$$\frac{dy}{dz} = g(x, y, z), \tag{6}$$

where $f = B_x/B_z$, $g = B_y/B_z$ with

$$B_x = -\frac{1}{9}y\left(\frac{1}{r_{\rm p}^2} + \frac{1}{r_{\rm c}^2}\right) - \frac{1}{9}\left(\frac{1}{r_{\rm c}^2} - \frac{1}{r_{\rm p}^2}\right) + \delta_{\rm T} e^{kx}\cos(kz), \tag{7}$$

$$B_y = \frac{1}{9}x\left(\frac{1}{r_{\rm p}^2} + \frac{1}{r_{\rm c}^2}\right), \tag{8}$$

and

$$B_z = 1 - \delta_{\rm T} e^{kx}\sin(kz). \tag{9}$$

Here $r_{\rm p}$ and $r_{\rm c}$ are given by (3) and (4), respectively, and $k = 1/3$.

3. Flux-preserving TWM

In this section, we derive an additional differential equation for the preservation of the magnetic flux for the TWM. The original two differential equations of the standard TWM plus this additional differential equation make the flux-preserving TWM. We then describe how we numerically solve the differential equations of the flux-preserving TWM. We also give a very brief summary of the LMN in this section since we compare some of the results from the flux-preserving TWM with the LMN.

3.1. Preservation of the magnetic flux

The critical property of the magnetic field is that it is divergence-free, $\nabla \cdot \mathbf{B} = 0$. This means that the trajectories of magnetic field lines are a single-degree-of-freedom, time-dependent Hamiltonian system [5, 6]. Hamiltonian systems are not generic in the set of dynamical systems, because Hamiltonian systems are not structurally stable against non-Hamiltonian perturbations. So the standard numerical schemes for integration of ordinary differential equations are not ideal for solving Hamiltonian equations. Numerical approximation introduces non-Hamiltonian perturbations giving a completely different long-term behavior. We can address this problem in a number of ways. One way is to use area-preserving maps [15, 16]. We can construct area-preserving maps by arranging each step of integration to be a canonical or symplectic transformation. Maps preserve the symplectic form. Preservation of the symplectic form is equivalent to preservation of the Poisson bracket operation. A consequence of the preservation of the operation of the Poisson bracket is Louiville's theorem. Discretization used in the construction of maps introduces a small non-integrable perturbation into the system [17]. The Kolmogorov–Arnold–Moser (KAM) theorem [18–20] tells us that most of the invariant tori will survive. In addition to these invariant tori, the perturbation will also create island chains surrounded by stochastic layers. If the system is close to being integrable, and has less than two degrees of freedom, then we know that there exist invariant tori that the trajectories cannot cross. So the energy of the system can only undergo

https://doi.org/10.1017/S0022377808007526 Published online by Cambridge University Press

bounded oscillations, and no Arnold diffusion can occur [18–20]. Another approach is to use numerical integrators that preserve the symplectic property [17]. We see then that preservation of the magnetic flux is equivalent to preservation of the symplectic form. Therefore, a third approach is to preserve the magnetic flux. This is the approach we adopt here. To accomplish the preservation of magnetic flux, we derive an additional differential equation to preserve the magnetic flux in the TWM.

3.2. Derivation of the additional differential equation for preservation of the magnetic flux

The magnetic field line equations in the Cartesian coordinates are $dx/dz = f(x, y, z)$ and $dy/dz = g(x, y, z)$ with $f(x, y, z) = B_x/B_z$ and $dy/dz = B_y/B_z$. Since the magnetic field is divergence-free, the magnetic flux $B_z J\delta x\delta z$ in an infinitesimal cell surrounding a field line trajectory must remain constant with J the coordinate Jacobian. The coordinates before and after a time step are $x_a = x_b + f(x_b, y_b, z_b)\delta z$ and $y_a = y_b + g(x_b, y_b, z_b)\delta z$. The coordinate Jacobian is

$$J \equiv \frac{\partial(x_a, y_a)}{\partial(x_b, y_b)} = 1 + \left(\frac{\partial f}{\partial x_b} + \frac{\partial g}{\partial y_b}\right)\delta z + (\cdots)(\delta z)^2. \tag{10}$$

That is, $dJ/dz = \partial f/\partial x_b + \partial g/\partial y_b$. Flux conservation says $(d/dz)(B_z J) = 0$, so the z component of the magnetic field along a field line trajectory obeys the differential equation

$$\frac{d\ln B_z}{dz} = -\left(\frac{\partial f}{\partial x} + \frac{\partial g}{\partial y}\right) = \frac{1}{B_z}\left(f\frac{\partial B_z}{\partial x} + \frac{\partial B_z}{\partial z}\right). \tag{11}$$

If one integrates this equation along with $dx/dz = f(x, y, z)$ and $dy/dz = g(x, y, z)$, then the extent to which the actual B_z at each point along the field line differs from that obtained by integration is a measure of the error in integration. We add this new differential equation (11) to the original set of two differential equations (5) and (6). We call the new set of differential equations, (5), (6) and (11), the flux-preserving TWM. This additional differential equation is an analytical expression for the preservation of magnetic flux, and it allows us to control the step size of numerical integration of the TWM equations to achieve desired accuracy in preservation of the magnetic flux.

3.3. Numerical implementation

We use the fourth-order Runge–Kutta scheme to integrate equations of the flux-preserving TWM. For a single run of the code, we keep the amplitude δ_T fixed. When we run the code, we do not fix how many field lines we will integrate since the code stops when 20 000 field lines from the stochastic layer hit the collector plate. We integrate each field line at the most for 10 000 toroidal circuits of the tokamak. We start the field lines at $x = 0$, $z = 0$, and $0 < y < y_{LGS}(\delta_T)$. Here $y_{LGS}(\delta_T)$ is the y coordinate of the last good surface where it intersects the y axis for a given δ_T. We use the new additional differential equation to control the accuracy of integration. We use the new equation to calculate the maximum step size Δz for integration. We calculate the actual B_z from $B_z = 1 - \delta_T \exp(kx)\sin(kz)$, and denote it by B_z^{actual}. We calculate B_z from numerical integration of (11), and denote it by B_z^{num}. The quantity $|(B_z^{\text{actual}} - B_z^{\text{num}})/B_z^{\text{actual}}|$ calculates the accuracy. We find that if $10^{-13} < \Delta z < 10^{-1}$, then the accuracy of the integration is in the range 10^{-9} to 10^{-7} for $0 < \delta_T \leqslant 10^{-3}$. Here Δz is the step size of the numerical integration. For

https://doi.org/10.1017/S0022377808007526 Published online by Cambridge University Press

the amplitude $\delta_T = 10^{-3}$, the step size is $10^{-1} > \Delta z > 10^{-13}$, and the tolerance τ is $10^{-9} \leqslant \tau \leqslant 10^{-7}$.

3.4. The LMN

We give a very brief description of the LMN. For details, see [21]. The LMN represents the effects of the naturally occurring low mn perturbation. We obtain the LMN by adding a term to the symmetric simple map (SSM) [22]. The SSM is derived by symmetrizing the simple map, and the simple map is the simplest area-preserving map that has topology of divertor tokamaks; just as the TWM is the simplest physical model that has topology of divertor tokamak. The SSM equations are

$$y_{n+1} = y_n + 2kx_n - 2k^2 y_n(1 - y_n), \tag{12}$$

$$x_{n+1} = x_n - ky_n(1 - y_n) - ky_{n+1}(1 - y_{n+1}). \tag{13}$$

We choose the SSM parameter $k = 0.3$. The edge safety factor, q_{edge}, for the SSM for $k = 0.3$ is 30. We take 10 iterations of the SSM to be equivalent to a single toroidal circuit of the tokamak, so the SSM with $k = 0.3$ represents a divertor tokamak with $q_{\text{edge}} = 3$ and O point at $(0, 0)$ and X point at $(0, 1)$. We place the divertor plate at $y = y_{\text{plate}} = 1$. In the SSM, the toroidal asymmetries can be simulated using the map parameter k, by additional terms, or by applying additional maps that explicitly include the effects of qualitatively different kinds of magnetic perturbations [22, 23]. The generating function that adds the effects of two quadrupoles of opposite helicity with toroidal mode numbers ± 1 is

$$\Delta(x, y) = \Delta_0 + \frac{1}{2}\delta_M(x^2 - y^2)\cos\left(\frac{2\pi i}{N_p}\right). \tag{14}$$

Here $\Delta_0(x, y)$ is the generating function for the SSM, i is the iteration number, N_p is the number of iterations of the unperturbed map that is equivalent to a single toroidal circuit of tokamak and δ_M is the amplitude of the low mn perturbation. Then, the LMN is given by the map equations

$$y_{n+1} = y_n + 2k(1 - \delta_n)x_n - 2k^2(1 - \delta_n)(1 - \delta_n - y_n)y_n, \tag{15}$$

$$x_{n+1} = x_n - ky_n(1 - \delta_n - y_n) - ky_{n+1}(1 - \delta_n - y_{n+1}). \tag{16}$$

Here $\delta_n = \delta_M \cos(2\pi n/N_p)$. The LMN is an explicit map. It preserves the topological invariance and is computationally efficient [21]. For $\delta_M = 0$, it reduces to the SSM. Here we have chosen the map parameter $k = 0.3$, amplitude $\delta_M = 10^{-3}$, and $N_p = 10$.

4. Results

Now we present the results from the flux-preserving TWM for the practically relevant, typical value of the amplitude $\delta = 10^{-3}$.

4.1. The phase portrait

In Fig. 1, we show a close view of the phase portrait near the X point for $\delta_T = 10^{-3}$. We see that the magnetic structure near the X point has a single, regular, large-scale structure. This structure is formed by the largest asymmetric term in the perturbation, the $n = 1$, $m = 1$ mode.

https://doi.org/10.1017/S0022377808007526 Published online by Cambridge University Press

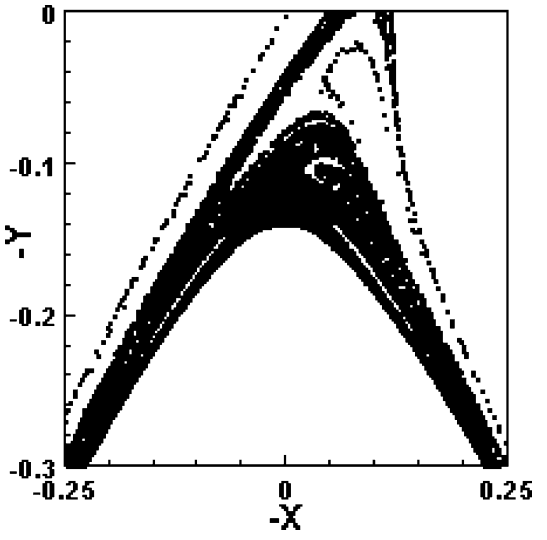

Figure 1. A close view of the stochastic layer near the X point in the Poincaré surface of section for $\delta_T = 10^{-3}$.

4.2. The width of the stochastic layer

To calculate the change in the width of the stochastic layer, w, as δ_T is varied, we fix δ_T, and start 10 000 field lines at $x_0 = 0$ and random y_0 distributed uniformly in the interval $(0, 1)$. We integrate each field line for at most 10 000 toroidal circuits of the tokamak. We consider a field line to be chaotic if it crosses the $y = 0$ plane before completing 10 000 toroidal circuits. We identify the chaotic line that is closest to the O point. Then, the distance from the starting position of this line on the y-axis and the X point is the width of the stochastic layer. We repeat this procedure for different values of δ_T. Using this procedure, we calculate the width of the stochastic layer as a function of amplitude of the perturbation.

In Fig. 2, we show $w(\delta_T)$. Overall, the width of the stochastic layer scales as $\delta_T^{0.38}$. We see that the width scales as: $w \propto \delta_T^{0.33}$ for $10^{-6} \leqslant \delta_T \leqslant 2 \times 10^{-5}$; $w \propto \delta_T^{0.037}$ for $3 \times 10^{-5} \leqslant \delta_T \leqslant 10^{-4}$; and $w \propto \delta_T^{0.49}$ for $10^{-4} \leqslant \delta_T \leqslant 10^{-3}$. So the flux-preserving TWM scaling of width is in very good agreement with Boozer–Rechester scaling [2] for typical levels of field errors [13–15]. Overall, in the TWM the exponent in the scaling of width is about 24% off from the Boozer–Rechester prediction. In Fig. 2, we also show the scaling of width with amplitude for the LMN. For the LMN, we iterate each field line for 100 000 toroidal circuits of the tokamak, and for a fixed δ_M, we integrate 10 000 field lines. For the LMN, the width scales as $\delta_M^{1/2}$. The scaling of width for the LMN is exactly in accordance with the Boozer–Rechester prediction. The width of the stochastic layer in the flux-preserving TWM is about an order of magnitude larger than the width in the LMN for the same values of the amplitude of perturbation.

From these results, we see that all three methods, the flux-preserving TWM, LMN and Boozer–Rechester, agree with the 0.5 power scaling of stochastic layer width with the amplitude of magnetic perturbation when the perturbation is sufficiently large. The flux-preserving TWM gives a larger stochastic layer width when the perturbation is small, but this may be due to numerical errors. For sufficiently

https://doi.org/10.1017/S0022377808007526 Published online by Cambridge University Press

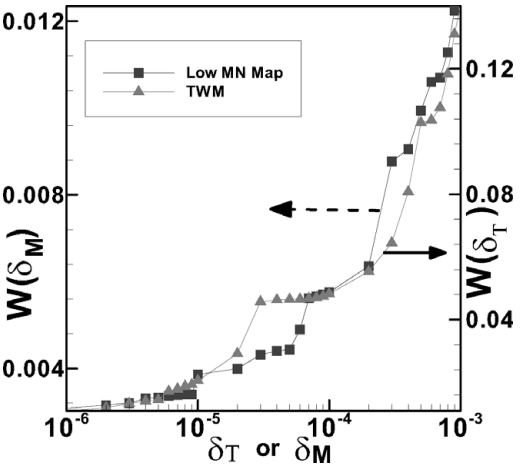

Figure 2. Dependence of the width of the stochastic layer on the perturbation amplitude. Results for the LMN are also shown.

small perturbations, the stochastic layer width will be dominated by numerical errors. For the smallest perturbations that we have considered, the numerical errors are only about 100 times smaller, so one could imagine that they produce a measurable enhancement of stochastic layer width. Boozer–Rechester scaling is an asymptotic, topological result. Despite the addition of an equation to the TWM for the preservation of magnetic flux, and despite the TWM being the simplest physical model that has the topology of the divertor tokamak, the flux-preserving TWM does not give correct scaling of the stochastic layer in this asymptotic region. The LMN does give correct scaling for small as well as large amplitudes.

4.3. Properties of the field lines in the stochastic layer

To calculate the properties of the field lines in the stochastic layer, we let $\delta_T = 10^{-3}$. We start 20 000 field lines in the stochastic layer near the X point, and integrate these lines for at most 10 000 toroidal circuits of the tokamak. If a field line crosses the $y = 0$ plane, we consider it as a chaotic line. Once a field line becomes chaotic, we do not integrate it any further. The safety factors, lengths, and toroidal and poloidal angles for these field lines are calculated.

The X point is located at $x = 0$, $y = 0$. For $\delta_T = 10^{-3}$, near the X point the last good confining surface passes through the point $x = 0$, $Y_{LGS} = 0.1399$, and the width of the stochastic layer is $w = 0.1399$. We start the field lines at $x = 0$, with $0 < y < Y_{LGS}$. We choose the y coordinates of the starting positions of field lines at random (with uniform distribution) in the stochastic layer. We express the starting positions of the field lines in terms of distance from the last good surface normalized by the width of the stochastic layer. We denote this distance by d.

In Figs 3, 4, 5, and 6, we show the safety factor, lengths of field lines, toroidal angles and the poloidal angles as functions of d. We see that in these figures the largest regular structures are the two structures corresponding to the leading asymmetries in perturbation, $n = 1$, $m = 1$ and 3. See also Sec. 4.4. Graphs in these figures show self-similar structures at smaller scales.

https://doi.org/10.1017/S0022377808007526 Published online by Cambridge University Press

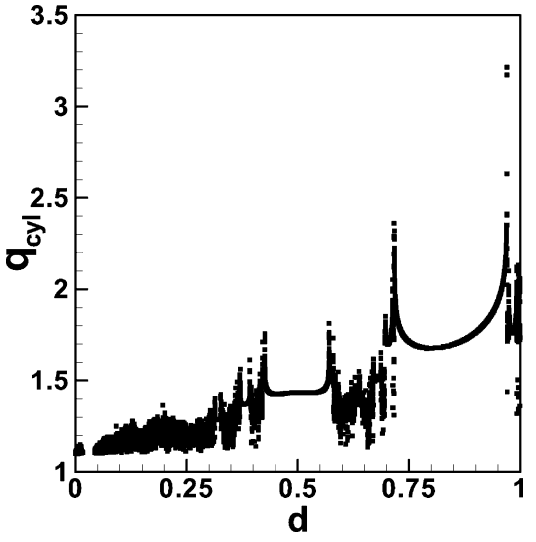

Figure 3. Safety factor q as a function of the starting position of field lines in the stochastic layer.

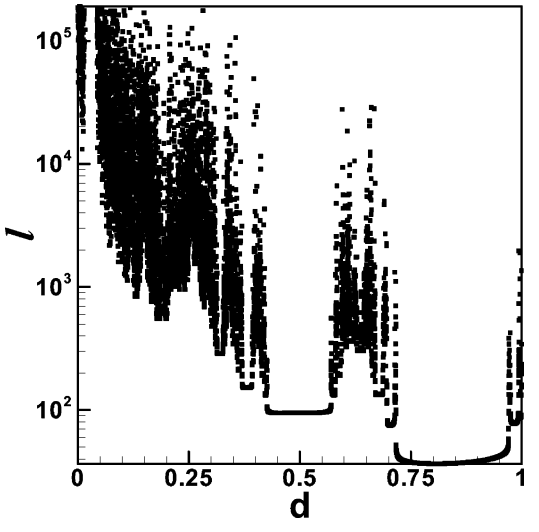

Figure 4. Lengths of field line l as a function of d.

4.4. Properties of the field lines in the magnetic footprint

Now we calculate the properties of the field lines in the magnetic footprint with $\delta_T = 10^{-3}$. We start field lines in the stochastic layer at $x = 0$, and $0 < y < Y_{LGS}$. We choose the starting y positions randomly with uniform distribution in the stochastic layer on the y-axis. We integrate each line at most for 10 000 toroidal circuits of the tokamak. We do not fix the number of lines that we are going to integrate when we start the code. We have designed the code to stop once 20 000 field lines hit the collector plate. The plate is located in the $y = 0$ plane. In an integration step if the y position of a field trajectory changes sign from positive to negative,

https://doi.org/10.1017/S0022377808007526 Published online by Cambridge University Press

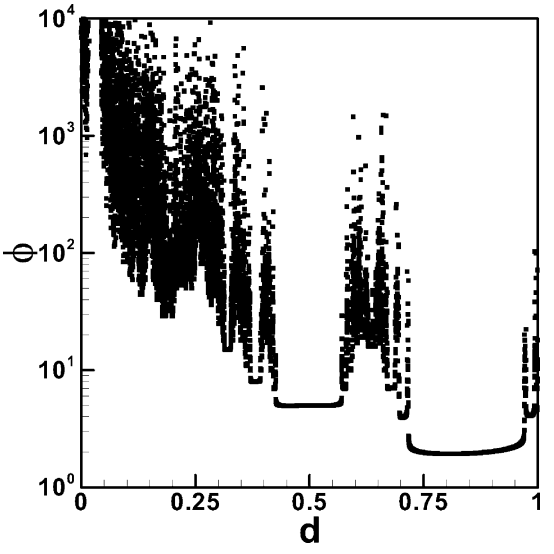

Figure 5. Toroidal angles φ as a function of d.

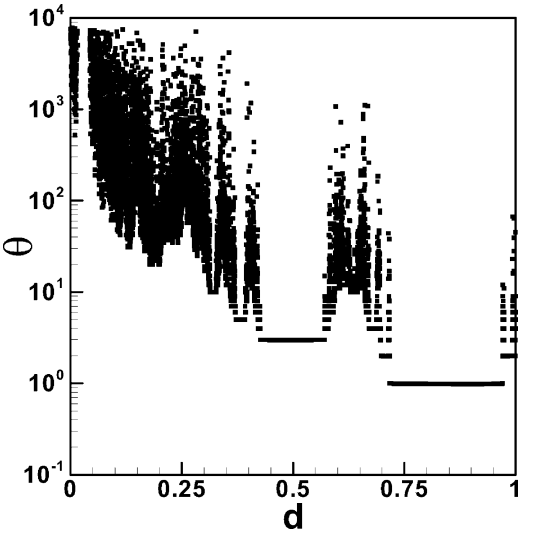

Figure 6. Poloidal angles θ as a function of d.

then that field line crosses the plate. At this step, we successively halve the step size until the difference in the y position of the trajectory and the plate is smaller than 10^{-6}. From this, we calculate the coordinates of the strike point of a line on the divertor plate. We denote the strike point by ($X_{\rm strk}$, $Z_{\rm strk}$). We express $Z_{\rm strk}$ in units of $2\pi R_0$. For each field line that strikes the plate, we also calculate the safety factor q, the semiconnection length l, toroidal angle φ, and the poloidal angle θ as functions of d. We divide these data into groups corresponding to the number of poloidal circuits that the field line makes before it hits the plate. We calculate the

https://doi.org/10.1017/S0022377808007526 Published online by Cambridge University Press

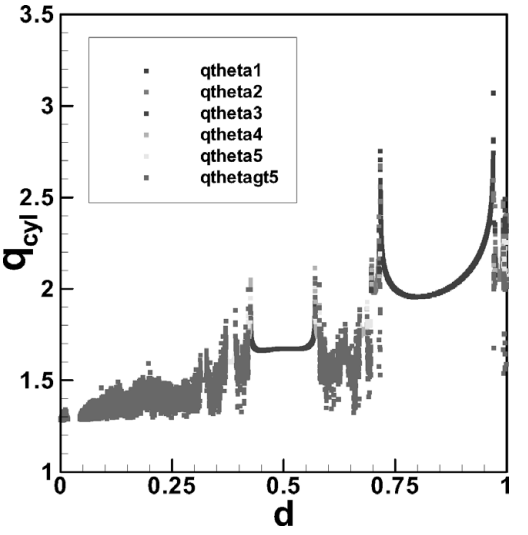

Figure 7. Dependence of safety factor q on the distance d from the last good surface for the lines that strike the plate.

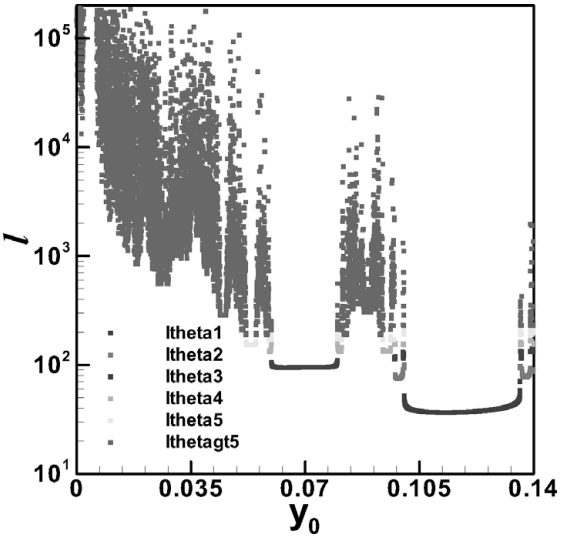

Figure 8. Dependence of semiconnection lengths l on the distance d from the last good surface for the lines that strike the plate.

area of the footprint using the method described in [15]. We show the results in Figs 7–11.

From Figs 7–9, we see that in the graphs of $q(d)$, $l(d)$, and $\varphi(d)$ two regular large-scale structures stand out inside the scatter of points. The larger of these two structures has $0 < \theta_{\text{strk}} \leqslant 1$, and the smaller has $2 < \theta_{\text{strk}} \leqslant 3$. From this we infer that the $n = 1$, $m = 1$ and 3 asymmetries in the perturbation create these structures. These structures are the footprint end of the field lines that bunch together spatially (toroidally and poloidally) and connect the stochastic layer to the material surface.

https://doi.org/10.1017/S0022377808007526 Published online by Cambridge University Press

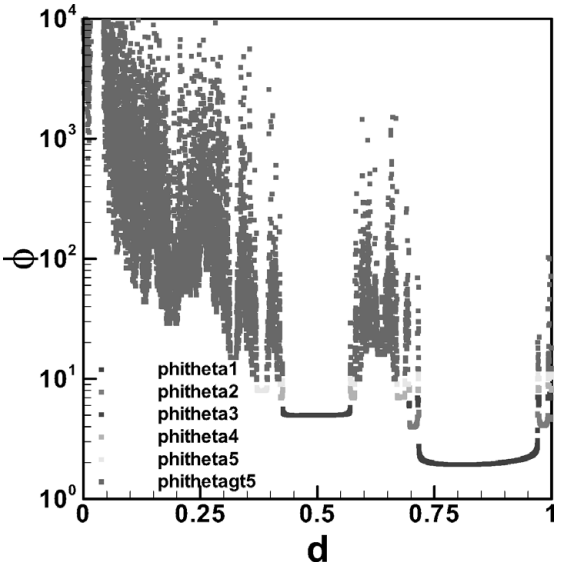

Figure 9. Dependence of the toroidal circuits made by the field lines on the distance d before striking the plate.

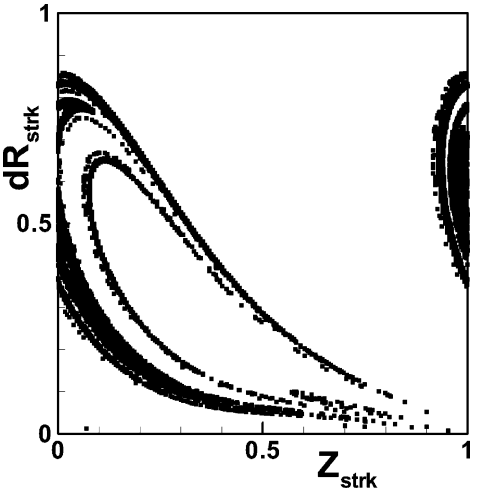

Figure 10. Magnetic footprint for the flux-preserving TWM with $\delta_{\mathrm{T}} = 10^{-3}$.

This spatial bunching of lines connecting the chaotic layer with the collector plate plays an important role in formation of regular structures in the footprint on the plate [24, 25].

In Figs 10 and 11, we show the magnetic footprints for the flux-preserving TWM and the LMN for $\delta_{\mathrm{T}} = \delta_{\mathrm{M}} = 10^{-3}$. In Figs 10 and 11, we express the transversal distance from the X points, dR_{SEP}, in units of width of the stochastic layer. For the flux-preserving TWM, we express the toroidal locations of the strike points, Z_{STRK}, in units of $2\pi R_0$, $R_0 = 3$; and for the LMN, the toroidal angular position of the strike points, φ_{STRK}, in units of 2π. Figures 10 and 11 show an important result. The

https://doi.org/10.1017/S0022377808007526 Published online by Cambridge University Press

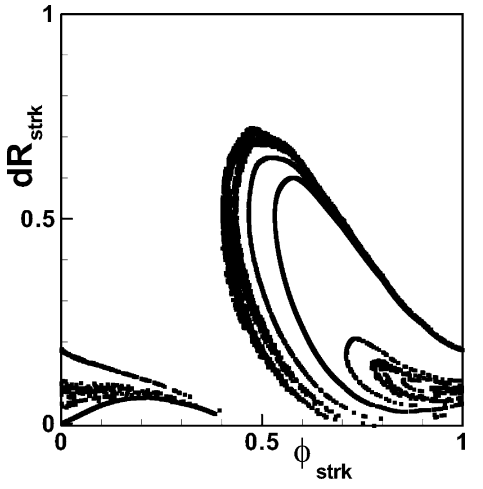

Figure 11. Magnetic footprint in the LMN map when $\delta_{\mathrm{M}} = 10^{-3}$.

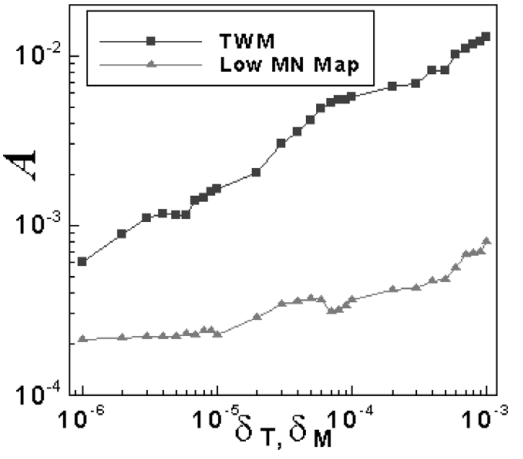

Figure 12. Comparison of the areas of magnetic footprints as a function of the amplitude of perturbation in the flux-preserving TWM and the LMN.

footprints for the flux-preserving TWM and the map show remarkable agreement in size (relative to the respective widths of stochastic layer), shape, and structure. In Fig. 12, we compare the dependence of the area of the footprint on the strength of the perturbation for the flux-preserving TWM with that of the map. Here we see good agreement between the flux-preserving TWM and the LMN except for some difference in the y scale.

4.5. Speed and accuracy

The maximum accuracy in the flux-preserving TWM is 10^{-9} for $0 \leqslant \delta_{\mathrm{T}} \leqslant 10^{-3}$. The maximum accuracy in the LMN is 10^{-14} for $0 \leqslant \delta_{\mathrm{M}} \leqslant 10^{-3}$. With these accuracies, the CPU time taken for 20 000 field lines to strike the plate after at most 10 000 toroidal circuits of the tokamak before striking the plate for the LMN is 1533 CPU seconds on a Dell Precision 340 work tower with a single Pentium 4 CPU. The CPU

https://doi.org/10.1017/S0022377808007526 Published online by Cambridge University Press

time for the flux-preserving TWM is 3774 CPU seconds. So the LMN is faster and more accurate.

5. Conclusions

We have added an equation to the TWM equations for divertor tokamaks. The additional equation allows the accuracy in the preservation of the magnetic flux in numerical integration of the TWM equations to be controlled. We call the TWM with the additional equation the flux-preserving TWM. Most of our results are for the typical levels of field errors. The phase portrait near the X point has a single, regular, large-scale magnetic structure corresponding to the $n=1$, $m=1$ mode. The Boozer–Rechester scaling is a topological result. The flux-preserving TWM, LMN, and Boozer–Rechester all agree with the 0.5 power scaling of stochastic layer width with the amplitude of the magnetic perturbation when the perturbation is sufficiently large. The flux-preserving TWM gives a larger stochastic layer width when the perturbation is small, but this may be due to numerical errors. For sufficiently small perturbations, the stochastic layer width will be dominated by numerical errors. For the smallest perturbations that we have considered, the numerical errors may produce a measurable enhancement of stochastic layer width. The deviation from the square root scaling does not seem to occur until we get below one part in 100 000. Changes in the safety factor, length, toroidal angle, and the poloidal angle with distance from the last good surface are calculated. This is done both for the stochastic layer and for the footprint. These graphs show self-similarities at smaller scales. The $n=1$, $m=1$ and 3 modes form the regular, large-scale structures seen in these graphs. These structures bunch the field line trajectories together toroidally and poloidally, and connect the stochastic layer to the plate. The magnetic footprint is a toroidally spiraling, large-scale structure. Footprints in the flux-preserving TWM and the LMN have a similar shape and structure, and are roughly the same size relative to the respective widths of the stochastic layer. The LMN preserves the topological invariance and also has the advantage of computational efficiency. So, for the analytic representation of field errors in the TWM, the structure and area of the magnetic footprint due to field errors in divertor tokamaks are largely formed by the asymmetric $n=1$, $m=1$ mode, and the magnetic perturbations with higher m numbers have a marginal effect on the magnetic footprint.

The flux-preserving TWM does not give correct scaling for small amplitudes, while the map gives correct scaling for all values of amplitude considered. So it is safer to use maps to integrate field lines rather than using numerical schemes such as the Runge–Kutta scheme. The reason this happens is that Hamiltonian systems are not generic in the set of dynamical systems. Hamiltonian systems are not structurally stable against non-Hamiltonian perturbations. Standard numerical schemes for integration of ordinary differential equations are not ideal for solving Hamiltonian equations. Numerical approximation introduces non-Hamiltonian perturbations giving a completely different long-term behavior. We can address this problem if we use maps for integration. Area-preserving maps preserve the features of Hamiltonian structure. If we arrange each step of integration to be a canonical or symplectic transformation, we get a map. Maps preserve the symplectic form. If the symplectic form is preserved, then it is mathematically equivalent to preservation of the operation of the Poisson bracket. A consequence of the latter

is Louiville's theorem [17]. The KAM theorem [18–20] tells us that most of the invariant tori will survive. In addition to these invariant tori, the perturbation will also create island chains surrounded by stochastic layers. If the system is close to being integrable, and has less than two degrees of freedom, then we know that there exist invariant tori that the trajectories cannot cross. The energy of the system can only undergo bounded oscillations, and no Arnold diffusion can occur [18–20]. TWM is the simplest model that has the topology of divertor tokamaks, and even for such a model, numerical integration schemes (with an extra equation for flux preservation) do not give us correct scaling for small amplitudes. So an estimate of the size of the stochastic layer and the footprint will also be off the mark. Maps preserve the Hamiltonian structure, and in addition have the advantages of computational efficiency and correct scaling of the stochastic layer.

In summary, here we have addressed the question of magnetic field structure in the vicinity of the separatrix in divertor tokamaks. We have investigated this problem earlier in a series of papers, using various mathematical techniques. In the present paper, we have studied the TWM. The TWM is the simplest physical model for divertor tokamaks. We have added an extra equation to the TWM. This equation expresses magnetic flux conservation in the TWM. This equation is derived from the TWM equations. So the equation does not add any new information to the TWM. The equation is useful in controlling the step size in the numerical integration of the TWM equations. Nevertheless, the technique is apparently still plagued by numerical inaccuracies when the perturbation level is low, resulting in an incorrect scaling of the stochastic layer width. Boozer–Rechester scaling is an asymptotic result, valid for small amplitudes. On the other hand, the map gives correct scaling for the entire range of amplitudes considered here. Maps respect the Hamiltonian structure. Maps are computationally fast. For a $1\frac{1}{2}$-degree-of-freedom Hamiltonian system such as field lines, maps also do not give Arnold diffusion.

Acknowledgement

This work is supported by the US DOE OFES under grants DE-FG02-01ER54624 and DE-FG02-04ER54793.

References

[1] Cordey, J. D., Goldston, R. J. and Parker, R. R. 1992 *Phys. Today* **45**(1), 22.
[2] Boozer, A. and Rechester, A. 1978 *Phys. Fluids* **21**, 682.
[3] Luxon, J. L. and Davis, L. E. 1985 *Fusion Technol.* **8**, 441.
[4] Evans, T. E. et al. 2006 *Nature Phys.* **2**, 419.
[5] Boozer, A. 1983 *Phys. Fluids* **26**, 1288.
[6] Cary, J. R. and Littlejohn, R. G. 1983 *Ann. Phys. (N.Y.)* **151**, 1.
[7] Post, D. E. et al. 1991 *ITER Documentation Series No. 21.* Vienna: IAEA.
[8] Reiman, A. 1996 *Phys. Plasmas* **3**, 906.
[9] Lau, Y. and Finn, J. 1991 *Astrophys. J.* **366**, 577.
[10] Stern, D. P. 1973 *J. Geophys. Res.* **78**, 7292.
[11] Greene, J. M. 1988 *J. Geophys. Res.* A **93**, 8583.
[12] Snipes, J. A., Campbell, D. J., Hender, T. C., Hellermann, M. V. and Weisen, H. 1990 *Nucl. Fusion* **30**, 205.
[13] Zohm, H., Kallenbach, A., Bruhns, H., Fussmann, G. and Klueber, O. 1990 *Europhys. Lett.* **11**, 745.

[14] LaHaye, R. J. and Scoville, J. T. 1991 *Rev. Sci. Instrum.* **62**, 2146.
[15] Punjabi, A., Verma, A. and Boozer, A. 1992 *Phys. Rev. Lett.* **69**, 3322.
[16] Punjabi, A., Ali, H., Evans, T. E. and Boozer, A. 2007 *Phys. Lett.* A **364**, 140.
[17] Cartwright, J. and Piro, O. 1992 *Int. J. Bifurcation Chaos* **2**, 427.
[18] Kolmogorov, A. N. 1954 *Dokl. Akad. Nauk SSSR* **98**, 527.
[19] Arnold, V. I. 1962 *Sov. Math. Dokl.* **3**, 136.
[20] Moser, J. 1962 *Nachr. Akad. Wiss. Gottingen, Math. Phys. K1* **12**, 1.
[21] Ali, H., Punjabi, A., Boozer, A. and Evans, T. E. 2004 *Phys. Plasmas* **11**, 1908.
[22] Punjabi, A., Ali, H. and Boozer, A. 1997 *Phys. Plasmas* **4**, 337.
[23] Punjabi, A., Ali, H. and Boozer, A. 2003 *Phys. Plasmas* **4**, 3992.
[24] Eich, T., Herrmann, A., Neuhauser, J. and the ASDEX Upgrade Team 2003 *Phys. Rev. Lett.* **91**, 195003.
[25] Eich, T. et al. *Plasma Phys. Control. Fusion* **47**, 815.